Visualizing ATP Dynamics in Live Mice

Norimichi Koitabashi[1, #], Riki Ogasawara[2, #], Ryuto Yasui[3, #], Yuki Sugiura[4], Hinako Matsuda[3, †], Shigenori Nonaka[5,6], Takashi Izumi[7], Masahiko Kurabayashi[1], Makoto Suematsu[4], Motoko Yanagita[3,8], Hiromi Imamura[9], Masamichi Yamamoto[10, 11, ‡, *]

[1]Department of Cardiovascular Medicine, [7]Department of Biochemistry, [10]Advanced Scientific Research Leaders Development Unit, Gunma University Graduate School of Medicine, Maebashi, Gunma 371-8511, Japan

[2]Department of Life Science and Applied Chemistry, Nagoya Institute of Technology, Gokiso-cho, Showa-ku Nagoya, Aichi 466-8555, Japan

[3]Department of Nephrology, Kyoto University Graduate School of Medicine, Kyoto University, Shogoin-Kawahara-cho, Sakyo-ku, Kyoto 606-8507, Japan

16 [4]Department of Biochemistry, Keio University School of Medicine, Shinamo-machi,

17 Shinjuku-ku, Tokyo 160-8582, Japan

18 [5] Spatiotemporal Regulations Group, Exploratory Research Center for Life and Living

19 Systems (ExCELLS), Nishigonaka 38, Myodaiji, Okazaki Aichi 444-8585, Japan

20 [6]Laboratory for Spaciotemporal Regulations, National Institute for Basic Biology

21 (NIBB)

22 [8]Institute for the Advanced Study of Human Biology (ASHBi), Kyoto University,

23 Yoshida-Konoe-cho, Sakyo-ku, Kyoto 606-8501, Japan

24 [9]Department of Molecular and Cell Physiology, Graduate School of Biostudies, Kyoto

25 University Yoshida-konoe, Sakyo ku, Kyoto 606-8501, Japan

26 [11]PRESTO, Japan Science and Technology Agency (JST), 4-1-8 Honcho Kawaguchi,

27 Saitama 332-0012, Japan

28 †Present address; Laboratory of Plant Gene Expression, Research Institute for

29 Sustainable Humanosphere, Kyoto University, Uji, Kyoto, 611-0011, Japan

‡Present address; Department of Nephrology, Kyoto University Graduate School of Medicine, Kyoto University, Shogoin-Kawahara-cho, Sakyo-ku, Kyoto 606-8507, Japan

#These authors contributed equally

Corresponding Author:

Masamichi Yamamoto, Ph.D.

myamamot@kuhp.kyoto-u.ac.jp, yamamoto.mailserver@gmail.com

Lead Contact

Masamichi Yamamoto

ABSTRACT

Analysis of the dynamics of adenosine triphosphate (ATP) is vital to quantitatively define the actual roles of ATP in biological activities. Here, we applied a genetically encoded Förster resonance energy transfer biosensor "GO-ATeam" and created a transgenic mouse model that allows systemic ATP levels to be quantitatively, sensitively, noninvasively, and spatiotemporally measured under physiological and pathological conditions. We used this model to readily conduct intravital imaging of ATP dynamics under three different conditions: during exercise, in all organs and cells; during myocardial infarction progression; and in response to the application of cardiotoxic drugs. These findings provide compelling evidence that the GO-ATeam mouse model is a powerful tool to investigate the multifarious functions of cellular ATP *in vivo* with unprecedented spatiotemporal resolution in real-time. This will inform predictions of molecular and morphological responses to perturbations of ATP levels, as well as the elucidation of physiological mechanisms that control ATP homeostasis.

58 **One Sentence Summary:**

59 Intravital real-time imaging of ATP dynamics in multiple organs using GO-ATeam

60 mice, can be used to quantitatively, sensitively, noninvasively, and spatiotemporally

61 measure systemic ATP levels and provide a platform for preclinical pharmacological

62 studies.

63

64

65 **Keywords**: Mice, ATP, Cardiotoxicity, Dynamics, Energy metabolism, Muscle

66 Contraction, FRET, Inter-organ network, Intravital, Imaging

67

68 **MAIN TEXT**

69

70 **INTRODUCTION**

71

72 Multiple recent technologies, including RNA-Seq, have driven considerable advances
73 toward a complete understanding and reliable prediction of biological activities at scales
74 ranging from single cells to whole organisms (Wang et al., 2009). However, much is yet
75 to be discovered regarding the coordinated and fluctuating biological activities in
76 multicellular organs under physiological and pathological conditions, as they impact
77 individual cells, because biological activities are regulated not only by intracellular
78 signals but also by extracellular signals and the environment. Biological activities such
79 as signal transduction, mRNA expression, and chromatin structure, as well as the
80 activities of the proteins that regulate these processes, are all affected by intracellular
81 adenosine triphosphate (ATP) levels (Fantl et al., 1993; Lusser and Kadonaga, 2003).
82 ATP is also fundamentally important for many vital cellular processes such as
83 maintaining the membrane potential and organelle transport in energy conversion

(Dzeja et al., 2002) (Dzeja et al., 2003) (Kamerlin et al., 2013) (Magistretti and Allaman, 2015) (Zala et al., 2013). Thus, a quantitative analysis of *in vivo* ATP dynamics at the single-cell level can provide a means for investigating the dynamics of biological activities in multicellular tissues. Such an analysis could address the question of whether ATP levels may vary between different cell types within the same tissue, for example, or how much fluctuation is normal between individual cells of the same type. Historically, it was impossible to measure ATP levels of tissues with classical biochemical methods while preserving the integrity of organs with high spatiotemporal resolution (Khlyntseva, 2009). In recent years, methods for detecting ATP via UV−visible absorption (Jung et al., 2017), magnetic resonance spectroscopy (Befroy et al., 2012) (Chaumeil et al., 2009)or nuclear magnetic resonance (Guo et al., 2014) have been developed, but none of these can quantify ATP concentrations with high resolution at the single-cell level. In 2009 two genetically encoded fluorescent biosensors, called Perceval (Berg et al., 2009) and ATeam (Imamura et al., 2009), were invented and enabled imaging of the ATP/ADP ratio and ATP within living culture cells, respectively. Later, improved ATP biosensors and other types of ATP biosensors were

reported, which include PercevalHR (Tantama et al., 2013), QUEEN (Yaginuma et al., 2014), MaLion (Arai et al., 2018), and GO-ATeam (Nakano et al., 2011). In this study, we chose a FRET-based ATP biosensor GO-ATeam, which employs green fluorescent protein as a donor and orange fluorescent protein as an acceptor, for studying ATP dynamics in living mammals. It is effective for these types of studies because of its minimal sensitivity to a broad pH range (6.3-8.3) and its ratiometric readout, which cancels fluctuation of fluorescent signals caused by movement of biological samples.

Here, we report the generation of an ATP visualization animal, “GO-ATeam mice”, in which the reporter achieve ubiquitous expression. Here we report our proof-of-principle analyses of different tissues and different methods. The ratio of FRET to GFP fluorescence intensities in intact cells was highly correlated with cytosolic ATP concentration determined by a proven biochemical method. These results prompted us to conduct imaging of live mice, for which we established GO-ATeam models of diverse physiological and pathological conditions. These findings support our expectation that GO-ATeam mice will serve as a useful platform for studying the dynamics of ATP *in vivo*, with the potential for conducting assays to elucidate the

maintenance of energy homeostasis in physiology and possibly preclinical pharmacological studies.

RESULTS

Generation of Transgenic Mice to Determine ATP Dynamics *In Vivo*

We chose to employ the GO-ATeam strategy (Nakano et al., 2011) to observe ATP dynamics in live mice. As noted above, this system employs GFP and OFP as the FRET pair, which can be readily detected and is minimally sensitive to pH, an important advantage because metabolic stress can cause a drop in intracellular pH. After several failed attempts to generate GO-ATeam transgenic mice, we obtained stable GO-ATeam knock-in mice with the FRET reporter cassette (**Figs. 1A-1H**). The knock-in mice yielded homozygous and heterozygous offspring consistent with Mendelian inheritance. Importantly, body weight, morphology and size, as well as the weights and functions of

the organs, were normal. Moreover, the mice were phenotypically normal throughout their expected lifespan of approximately three years (data not shown).

The FRET/GFP Ratio Reliably Reflects Cytosolic ATP Concentrations in GO-ATeam Mice

To examine whether the GO-ATeam probe can effectively measure cytosolic ATP concentrations in GO-ATeam knock-in mice, we first investigated the fluorescence signals in mouse embryonic fibroblasts (MEFs) obtained from GO-ATeam knock-in mice. After permeabilization of the plasma membrane of MEFs (n = 37), we recorded FRET/GFP ratios in the cells with a two-photon microscope while stepwise increasing the ATP concentrations in the medium (**Figs. 1A-1D**). The intracellular FRET/GFP ratio changed as a function of applied ATP concentration, ranging from 0.1 mM to 6 mM. By fitting the dose-response plot with the Hill equation, we obtained a calibration curve for directly estimating ATP concentrations from the FRET/GFP ratios (**Fig. 1I**).

To further validate the FRET/GFP ratio as a quantitative measure of ATP concentration, we treated two-cell-stage embryos from knock-in mice with 2-deoxy-D-glucose to inhibit glycolysis, and antimycin A to inhibit OXPHOS, followed by

147 estimations of ATP concentrations at certain time points either with fluorescence-based
148 FRET imaging (**Figs. 1E-1H**, n = 16) or with a proven cell lysate-based firefly
149 luciferase method (n = 118). The time-course of ATP change estimated by FRET
150 imaging was virtually superimposable with the time-course obtained by the luciferase
151 method (R^2 = 0.9846) (**Fig. 1J**). Thus, we concluded that cytosolic ATP concentrations
152 in living cells from GO-ATeam mice can be reliably estimated by imaging with a two-
153 photon microscope.

154 We next examined whether the expression level of the GO-ATeam probe in the knock-
155 in mice is sufficient for the quantitative measurement of FRET signals. To assess the
156 sensitivity and accuracy of GO-ATeam FRET/GFP ratio measurements, we generated
157 embryos expressing different levels of GO-ATeam2 by electroporating wild-type
158 single-cell embryos with GO-ATeam2 mRNA (n = 756), and compared the estimated
159 ATP concentrations from FRET/GFP ratios of the embryos acquired at 16 bits with a
160 two-photon microscope (**Fig. S2,** red dots). The total average autofluorescence
161 intensities of the embryos were 1389 ± 1.65 (n = 36). As expected, the estimated ATP
162 concentrations of embryos showing low average fluorescence intensities varied widely.

In contrast, those showing high average fluorescence intensities (>10,000 , at least 7-fold higher than the autofluorescence intensities) were within a relatively narrow range (2.40 ± 0.01 mM), which were very close to the ATP concentration obtained from the luciferase assay (2.34 ± 0.06 mM, n = 49). The total average fluorescence intensities of all heterozygous and homozygous knock-in embryos were more than 10,000, and more than 7-fold higher than the autofluorescence intensities, indicating that the ATP level could be calculated accurately for these embryos. It should be added that the homozygous knock-in embryos had an average fluorescence intensity value of about twice that of the heterozygous knock-in embryos (n = 88 and n = 68, blue dots and green dots in Fig. S2, respectively). Therefore, as a rule, we accepted measurements with total average fluorescence intensities that were more than 7x the autofluorescence intensities in the analyses that follow.

In addition to a two-photon microscope, we also employed a fluorescence stereo microscope, which can capture low magnified features in the bodies. Fig. S1A-D shows the same images of liver slices from GO-ATeam mouse in normoxic and hypoxic conditions captured by a two-photon microscope and a fluorescence stereo microscope

(**Figs. S1A–S1D**). The FRET/GFP ratios of the low magnified images were closely correlated with those of the two-photon micrographs (R^2 = 0.92, n = 139, **Fig. S1E**), indicating that a fluorescence stereo microscope can be used for quantitative estimation of ATP levels in GO-ATeam mice at a low magnified scale.

Differences in ATP Concentrations in Multiple Organs and Cell Types

In order to explore the heterogeneity in ATP concentrations within and between organs, we analyzed ATP levels in live neonatal (postnatal day 0) and adult (8 weeks of age) GO-ATeam mice. First, the animals underwent laparotomy after anesthesia, followed by imaging with a stereo microscope. The FRET/GFP images of the neonate (**Figs. 2A,B**) and those of the adult (**Fig. S3A**) revealed clear differences in ATP levels between organs. For example, brown adipose tissues, which were located between the shoulders, showed significantly lower FRET/GFP ratios compared with surrounding tissues (**Fig. 2A**). ATP concentrations of heart, lung, liver, kidney, pancreas, stomach, small intestine, and large intestine, which were estimated from fluorescence images, ranged approximately from 1 to 6 mM (**Fig.2C-J**, right column). We also estimated ATP

195 concentrations of these organs using a firefly luciferase method (**Fig. 2C-J**, left
196 column), and found that the values were roughly similar to those estimated from
197 fluorescence images, except for the large intestine, although there was large variance in
198 luciferase-based ATP concentrations. Because the penetration of the excitation light of
199 the microscope into surface tissues steeply decreases, the stereo microscope only detects
200 fluorescent signals from the surface of organs, while the luciferase method measures
201 ATP in the whole organ. Thus, the large difference in estimated ATP concentrations of
202 the large intestine observed between the two methods might suggest large variations in
203 ATP concentrations within the organ; i.e., higher ATP in the muscle layer of the
204 intestine, and lower ATP in the luminal tissues, such as villus. It is suggested that large
205 variance is influenced by the time from organ harvest to luciferase assay and the
206 efficiency of organ crushing.

207 Next, we performed two-photon intravital FRET/GFP imaging to detect ATP in the
208 deep tissues and cells of adult and neonatal GO-ATeam mice, which were anesthetized
209 using intratracheal intubation. The analyses of adult (**Figs. 2K–2Y**) and neonatal (**Figs.**
210 **S3J–S3O**) GO-ATeam mice included the following organs: liver (**Figs. 2K, 2L, and**

211 **S3J**); kidney (**Figs. 2M, S3M, and S3N**); small intestine (**Figs. 2N, 2O, S3K, and**

212 **S3L**); large intestine (**Figs. 2P and 2Q**); spleen (**Figs. 2R and 2S**); pancreas (**Figs. 2T,**

213 **2U, and S3O**; and skin (**Figs. 2V–2Y**). The images reveal striking differences in ATP

214 concentrations among organs and cells.

215

216

217 **ATP Dynamics Associated with the Force Generated by Muscle Contraction**

218 The role of ATP in fueling muscle contraction has been intensively studied for decades,

219 mainly through investigations of small animals and only a few muscle types **(Barclay,**

220 **2017) (Barclay, 2015)**. However, it still unknown to what extent these previous studies

221 on tissues, isolated muscle, or muscle cells—reflect the ATP dynamics in additional

222 muscle types and other mammalian species with varying energy needs, because live

223 animal imaging has not been exploited **(Barclay, 2015)**. *In vivo* analyses of ATP

224 dynamics will likely enhance our understanding of the linkage between bioenergetics

225 and muscle contraction. We began our *in vivo* approach by using GO-ATeam mice to

226 study ATP dynamics associated with the force generated by muscle contraction.

For this purpose, we immobilized the legs of live mice and electrically stimulated the sciatic nerve to induce contractions of the tibialis anterior muscle (**Fig. S4A**). FRET/GFP ratios in the tibialis anterior muscle were recorded with the fluorescent stereo microscope (**Figs. 3A-J**), simultaneously with torques generated by the muscle contraction; a range of responses was generated by stimulating the sciatic nerve with various frequencies. The muscle underwent twitching constriction at 20 Hz stimulation, while tetanic constriction was observed at 100 Hz stimulation. After applying stimulation, immediate increases and decreases in torques (**Fig. 3K**) and FRET/GFP ratios (n = 4, **Fig. 3L**) were observed, respectively. Maximum torque was generated within 0.9 s upon 100 Hz stimulation (**Fig. 3K**). The usage of ATP expeditiously increased then decreased, even the peak torque was still being produced (**Fig. S4B**), implying that the production of force may become more efficient once muscle is maximally contracted. (Jones et al., 2009) reported that the ATP level present in all skeletal muscles before and after contractile motion is unchanged when examined by the firefly luciferase method. However, when the identical type of anterior cervical muscle was measured before and after contraction using the ATP visualization mouse

243 technique, the ATP level decreased with contraction (**Fig. 3**). The effect was subtle, as
244 the ATP level decreased by only 0.6 mM even at 100 Hz exercise. These results suggest
245 that the firefly luciferase method did not detect the decrease in ATP levels due to
246 limitations of the experimental technique. The changes in both the torques and
247 FRET/GFP ratio were highly dependent on the frequency of the applied stimulations.
248 The simultaneous measurement of ATP levels and torque in real time showed that
249 considerable amounts of ATP were consumed when generating torque, and that while
250 maintaining torque the same amount of ATP was used regardless of the magnitude of
251 the torque. These results demonstrate the utility of the GO-ATeam mouse for
252 quantitative evaluations of energy efficiency in muscle strength (i.e. torque) of various
253 muscles; in addition, it will help to clarify the differences between sarcomeres that
254 occur unevenly in muscle cells, and which might vary with the distribution and timing
255 of energy use.
256
257 **The GO-ATeam Reporter Facilitates Studies of the Local and Peripheral Effects of**
258 **an Acute Pathological Insult**

We next sought to determine whether GO-ATeam mice serve as an accurate and sensitive reporter of the local and global effects on ATP dynamics of an acute pathological insult of major medical significance. We were particularly interested in our ability to monitor ATP dynamics in organs and tissues peripheral to the primary site of pathology, because such information may aid in diagnosis at early stages of disease that are otherwise difficult to detect. In humans, the heart is the organ that consumes the most ATP, and ischemic heart disease is the leading cause of death worldwide (Opie, 2003). We created a myocardial infarction model by ligating the left anterior descending artery (LAD) in GO-ATeam mice. We acquired intravital images of ATP dynamics in sham-operated (n = 8) (**Figs. 4A, 4C, 4E, S5A, and S5C**) and experimental mice (n = 8) (**Figs. 4B, 4D, 4F, S5B, and S5D**) 5 days after the procedure. At this time, echocardiography revealed marked left ventricular dysfunction with focal hypokinesis and enlargement of the heart chamber, and histology revealed the infarction scar (data not shown) at the anterior wall. Intravital FRET/GFP imaging showed that ATP concentration was clearly diminished in the ischemic region of the LV, as well as in other organs such as the liver, large intestine, kidneys, and small intestine (**Figs. 4B,**

275 **4D, 4F, S5B, D**). On the other hand, ATP levels increased around the ischemic region
276 of the LV. This increase in ATP levels within the "border zone" is consistent with the
277 fact that energy charge rises around the infarct lesion which was previously shown in
278 heart and brain ischemia models using imaging mass spectrometry(Hattori et al., 2010)
279 (Sugiura et al., 2016). These results indicate that the use of GO-ATeam mice can be
280 used to analyze the ATP dynamics throughout the body on a time scale up to several
281 days.

282 We next used the stereo microscope to perform time-lapse imaging of the whole
283 body immediately after the LAD ligation to examine minute-scale changes in the whole
284 body during acute heart failure induced by myocardial infarction. We found that the
285 ATP levels in the liver (n = 6) (**Figs. 4G–4G" and 4I**) and kidney (n = 4) (**Figs. S5E–**
286 **5E"**) started to decrease ($P < 0.05$) after 31 min and 32 min after LAD ligation,
287 respectively. ATP levels in the large intestine (n = 6) (**Figs. 4H–4H" and 4J**) and small
288 intestine (n = 6) (**Figs. S5F–5F" and S5I**) started to decrease ($P < 0.05$) much earlier,
289 13 min and 12 min minutes after LAD ligation, respectively. Blood flow in the liver
290 decreased by approximately 60% after ligation of the LAD (data not shown). These

291 results indicate that GO-ATeam mice can be used to analyze global effects on ATP
292 dynamics in response to acute pathological insults.

293 Next, we used two-photon microscopy to investigate the LAD ligation-induced
294 alterations in ATP dynamics of organs at the cellular level. We found that ATP levels
295 after 10 min only decreased around the pericentral regions in the liver (**Figs. 4K–K"**
296 **and 4M**; ROI 2, red), while ATP levels were maintained along the periphery of the
297 interlobular region including periportal regions (**Figs. 4K–K" and 4M**; ROI 1, blue) ,
298 showing intralobular heterogeneity in ATP drop in response to hypovolemic hypoxia.
299 This observation is consistent with the previous report showing greater susceptibility of
300 pericentral regions to hypoxia (Suematsu et al., 1992a; Suematsu et al., 1992b). In the
301 large intestine, ATP levels gradually decreased in the large intestinal glands and lamina
302 propria (**Figs. 4L–L" and 4N**; ROIs 1, 2 and 3, blue, red and orange). Glands tended to
303 maintain ATP levels compared with the lamina propria. These results demonstrate that
304 there is a large intercellular heterogeneity in the reduction of ATP during hypoperfusion
305 and hypoxia, even within the same organ, in real-time analysis. Clinically, for example,
306 hepatocyte necrosis is observed near the central vein on a time scale of days after

307 myocardial infarction. Therefore, although the time scales are different, these data show
308 the order and area of ATP reduction in each of these organs correlates with clinical
309 information on organ abnormalities and necrosis during myocardial infarction
310 (Sherlock, 1951).

311 We also detected a decrease in the amount of ATP within a limited region near a
312 central vein in the liver by mass spectrometry imaging 20 min after LAD ligation (**Figs.**
313 **4P**), consistent with the above FRET observation. In contrast, metabolome analysis of a
314 whole liver did not detect the ATP decrease at the same time point (Fig. 4O). Thus,
315 ATP imaging using GO-ATeam mice can detect local bioenergetic changes in real time
316 with high sensitivity.

317

318 **Assessment of Drug-Induced Cardiotoxicity in GO-ATeam2 Mice**

319 Drug-induced cardiotoxicity is a significant safety issue in drug development
320 because it can be fatal (Watkins, 2011). However, cardiotoxicity may become apparent
321 after clinical trials and marketing, and risk assessment in nonclinical trials has been
322 difficult.

323 The mouse heart contracts and relaxes about seven times per second using a large
324 amount of ATP. This exquisite balance between supply and consumption keeps the
325 amount of ATP in the cytoplasm of cardiomyocyte constant. However, if the balance is
326 slightly disturbed due to the toxicity of a drug to the heart, ATP concentrations will
327 change within a short time. Thus, we hypothesized that cardiotoxicity of a drug may be
328 detected as a change in the ATP dynamics of the heart before a change appears on the
329 electrocardiogram, etc.(**Fig. 5A**). To test this, we examined anticancer drugs with
330 reported cardiotoxicity, antiarrhythmic drugs and antibiotics that induce torsade point
331 (TdP).

332 Cardiac ATP levels were observed for 1 hour using a fluorescence stereo
333 microscope while the drug was continuously administered via the jugular vein at
334 concentrations that did not elicit an abnormal electrocardiogram (**Figs. 5B, C**).
335 Examination of the time-course changes in the ATP level in the heart immediately
336 before administration showed that there was almost no change in physiological saline
337 (n= 10) and furosemide (n=9), a diuretic with no cardiotoxicity, with a rise of about
338 0.05-0.1 mM, consistent with the data shown in **Fig. 1** (**Figs. 5D and E**). In contrast,

339 administration of doxorubicin (an anthracycline anticancer drug, n=3) , 5-FU (an
340 antimetabolite anticancer drug, n=6), and cyclophosphamide (an alkylating agent, n=4),
341 rapidly reduced ATP levels, which then recovered (**Figs. 5F, S6A and S6B**). This is
342 consistent with reports that doxorubicin accumulates in mitochondria in
343 cardiomyocytes, causing increased oxidative stress and mitochondrial dysfunction
344 (Ichikawa et al., 2014; Zhang et al., 2012). It is also consistent with clinical reports that
345 5-FU causes transient coronary vasospasm and cardiac ischemia, and that
346 cyclophosphamide causes myocardial damage (Schimmel et al., 2004). On the other
347 hand, when the alkylating agent ifosfamide was administered, the ATP level decreased
348 only moderately in the entire heart, but the ATP level decreased significantly only in the
349 left ventricle (**Fig. 5G**, n=5). This is consistent with clinical reports of ifosfamide
350 eliciting left ventricular dysfunction (Cardinale et al., 2000). These results suggest that
351 the cardiotoxicity of each anticancer drug can be detected as a change in ATP dynamics,
352 adding consistent molecular evidence to clinical reports.
353 In addition to anticancer drugs, we evaluated the drug-induced TdP, a fatal ventricular
354 arrhythmia as a measure of cardiotoxicity. TdP has been a significant safety issue in

355 drug development; current predictions of TdP in non-clinical trials are not fully

356 consistent with clinical TdP inducibility (Laverty et al., 2011).

357 We hypothesized that energy abnormalities might be related to myocardial electrical

358 instability. Therefore, GO-ATeam2 mice were used to determine whether the results of

359 the comprehensive *in vitro* proarrhythmia assay CiPA (Strauss et al., 2019) could be

360 improved. First, the antiarrhythmic drugs disopyramide, procainamide, nifekalant,

361 verapamil, and vanoxerine were examined (**Figs. 5H-J, 5M and S6C**). Disopyramide

362 has been reported to reduce myocardial contractility by blocking Na^+ channels (Mathur,

363 1972). The administration of TdP-inducing antiarrhythmic drugs disopyramide,

364 procainamide and nifekalant all increased the ATP level in the heart by 0.25 mM or

365 more by continuous administration for 60 minutes (**Figs. 5H, I, S6C**, n=6, 6, 5). On the

366 other hand, verapamil, an antiarrhythmic drug that blocks hERG channels but

367 suppresses TdP, showed little change in ATP levels (**Fig. 5J**, n=6) (Milberg et al., 2005

368 124). Similarly, vanoxerine, which blocks hERG channels but does not affect QT

369 prolongation in the heart, did not alter ATP levels (**Fig. 5M**, n=4) (Lacerda et al., 2010).

370 Next, antibiotics and antifungals such as levofloxacin, erythromycin, amphotericin B,

azithromycin, ciprofloxacin, and metronidazole were examined (**Figs. 5K, S6E-I**, n=5, 7, 4, 5, 5, 3). As with antiarrhythmic drugs, continuous administration for 60 minutes increased the intracardiac ATP level by 0.25 mM or more for all antibiotics and antifungals, despite having different actions and chemical structures (**Figs. 5K, S6E-I**, data not shown). Furthermore, continuous administration of alfuzosin (n=5), a prodrug for inducing TdP, and droperidol (n=9), an antipsychotic, increased intracardiac ATP levels by 0.25 mM or more by continuous administration for 60 minutes (**Figs. 5L, S6**). Of the approximately 60 TdP-inducing drugs registered with the FDA, all 11 that we tested raised ATP levels by 0.25 mM or more by continuous administration for 60 minutes. These results indicate that the GO-ATeam mouse model can reliably identify drugs that induce TdP based on changes in the amount of cellular ATP.

DISCUSSION

Adaptable to Other Imaging Technologies

386 In the GO-ATeam2 mouse model, identification of cell types and observation of cell
387 morphology can be observed by expressing far-red fluorescent proteins with different
388 spectra, such as mCardinal (Chu et al., 2014) and mRaspberry (Wang et al., 2004), in
389 the nucleus and cell membrane. A chemical dye can provide the fluorescent signal for a
390 third color. Specific cell labeling using DiD and ER labeling using ER-Tracker Blue-
391 White DPX can also be performed. ATP levels can also can be monitored
392 simultaneously with the fluctuation of mitochondrial mass using MitoTracker DeepRed.
393 Since the GO-ATeam mouse model can be used for a simple allele knock-in of GO-
394 ATeam2, it can be similarly modified by crossing with other transgenic mice and
395 various genetically modified mice. Examples include the GO-ATeam Amyotrophic
396 lateral sclerosis model and the heart failure model.
397 In the GO-ATeam mouse model, spatiotemporal information on ATP dynamics is
398 obtained from the organ level to the cell level in the whole mouse within the same
399 individual after the onset of the disease (myocardial infarction) or after drug
400 administration. It can be applied not only to intravital imaging but also to ATP

401 dynamic observation under various conditions such as *ex vivo* and primary cultured

402 cells, such as organ slices.

403

404 **Indicator of ATP Levels**

405 Cellular ATP levels and ATP sensing are integral to an assortment of regulatory

406 processes, including phosphorylation of signaling molecules, epigenetic factors,

407 chromatin remodeling factors, and activation of ion pumps (Lusser and Kadonaga,

408 2003) (Fantl et al., 1993) (Skou, 1965) (Becker and Horz, 2002). Feedback mechanisms

409 can influence enzymatic activity in response to changes in ATP concentration. Thus,

410 fluctuations in ATP levels are can indicate a change in an organ or cell function that is

411 not simply correlated with the amount of these proteins. Turning this around, knowing

412 how ATP concentrations affect biochemical enzymatic activities may allow the direct

413 measurement of ATP levels to serve as a proxy for biochemical assays. This implies

414 that if ATP dynamics are quantified in real time, *in vivo*, spatiotemporal information

415 related to functional changes can be obtained at the cellular level. For example, in

416 cortical neurons, ATP levels are involved in the depth of the resting membrane potential

417 and control nerve firing, because ATP is required for ion pumps, and the ATP
418 concentration correlates with ion pump activity (manuscript in preparation). It will be
419 interesting to compare ATP levels with gene expression profiles obtained from
420 comprehensive analyses such as RNA-Seq at the cell level, and correlate these with
421 spatiotemporal information. We presume that the main cellular factors controlled by the
422 ATP level differ depending on the organ in question, cell type, and the environment.
423 However, it is necessary for the near future to clarify these major factors by artificially
424 increasing or decreasing ATP levels at the cellular level *in vivo*.
425

426 **A model for evaluating drug effects on ATP homeostasis in living animal**

427 In general, ATP levels in the cytoplasm are always kept constant by balancing between
428 consumption and supply in living cells (Ingwall, 2004). On the other hand, if there is a
429 spatiotemporal perturbation of the consumption/supply balance, the ATP levels in the
430 cytoplasm are expected to change. Glycolysis and OXPHOS are responsible for the
431 generation of ATP. However, OXPHOS is much more efficient at ATP production than
432 glycolysis, so most ATP production in normal cells depends on OXPHOS. If the ATP

supply from OXPHOS decreases due to functional decline, such as mitochondrial injury, the supply is temporarily compensated for by using ATP reserves inside the cell, and ATP consumption is reduced. Subsequently, the body maintains homeostasis by activating the glycolysis system to restore the total supply of ATP and rebalance the energy homeostasis. (Ingwall, 2009). In the initial stage of heart disease, either metabolic stress (e.g., ischemia) or mechanical overload (e.g., pressure-overload) alters the ATP homeostasis (Kolwicz et al., 2013). Long-term metabolic stress to maintain an appropriate intracellular ATP level as above leads to cellular dysfunction, cell death, and heart failure (Kolwicz et al., 2013). To understand this progression, monitoring the spatiotemporal changes in ATP levels would be informative. In addition, for anti-cancer drug-induced cardiomyopathy, ATP homeostasis and mitochondrial function are key as well (Wallace et al., 2020). As a proof of principle, ATP visualization experiments with drug administration were performed here. All the drugs tested to induce cardiotoxicity also changed ATP levels in the heart in a short time, as observed with GO-ATeam FRET (**Fig. 5, S6**). We speculate that anti-cancer drugs appear to decrease cardiac ATP production due to mitochondrial damage. The mitochondrial damage and decreased

449 OXPHOS may increase myocardial oxidative stress and irreversible damage in late
450 phases of anti-cancer treatment (Wallace et al., 2020). ATP changes elicited by
451 antiarrhythmic drugs are qualitatively as well as quantitatively different from those
452 produced by anticancer drugs. Antiarrhythmic drugs cause “negative inotropic effects”
453 of contractile proteins, thereby reducing ATP consumption. Since ATP imaging reflects
454 the difference between ATP production and consumption, ATP imaging in the beating
455 heart showed that the intracellular ATP level increases in response to antiarrhythmic
456 drug administration. Conceivably, ATP production from mitochondria might be
457 increased by anti-arrhythmic drugs, although the hypothetical mechanism is unknown.
458 In any case, the increase in the intracellular ATP level may lower the membrane
459 potential and thereby cause an arrhythmogenic effect.
460 Our data show that GO-ATeam mice can elucidate physiological phenomena by
461 accurately measuring ATP levels over time in the cells and tissues *in vivo*. The GO-
462 ATeam system can potentially be extended to a wide range of applications, such as
463 elucidating networks between organs throughout the body and assessing toxicity.
464

References and Notes:

Arai, S., Kriszt, R., Harada, K., Looi, L.S., Matsuda, S., Wongso, D., Suo, S., Ishiura, S., Tseng, Y.H., Raghunath, M., *et al.* (2018). RGB-Color Intensiometric Indicators to Visualize Spatiotemporal Dynamics of ATP in Single Cells. Angew Chem Int Ed Engl *57*, 10873-10878.

Barclay, C.J. (2015). Energetics of contraction. Compr Physiol *5*, 961-995.

Barclay, C.J. (2017). Energy demand and supply in human skeletal muscle. J Muscle Res Cell Motil *38*, 143-155.

Becker, P.B., and Horz, W. (2002). ATP-dependent nucleosome remodeling. Annu Rev Biochem *71*, 247-273.

Befroy, D.E., Rothman, D.L., Petersen, K.F., and Shulman, G.I. (2012). (3)(1)P-magnetization transfer magnetic resonance spectroscopy measurements of in vivo metabolism. Diabetes *61*, 2669-2678.

Benabdellah, F., Touboul, D., Brunelle, A., and Laprevote, O. (2009). In situ primary metabolites localization on a rat brain section by chemical mass spectrometry imaging. Anal Chem *81*, 5557-5560.

Berg, J., Hung, Y.P., and Yellen, G. (2009). A genetically encoded fluorescent reporter of ATP:ADP ratio. Nat Methods *6*, 161-166.

Cardinale, D., Sandri, M.T., Martinoni, A., Tricca, A., Civelli, M., Lamantia, G., Cinieri, S., Martinelli, G., Cipolla, C.M., and Fiorentini, C. (2000). Left ventricular dysfunction predicted by early troponin I release after high-dose chemotherapy. J Am Coll Cardiol *36*, 517-522.

Chaumeil, M.M., Valette, J., Guillermier, M., Brouillet, E., Boumezbeur, F., Herard, A.S., Bloch, G., Hantraye, P., and Lebon, V. (2009). Multimodal neuroimaging provides a highly consistent picture of energy metabolism, validating 31P MRS for measuring brain ATP synthesis. Proc Natl Acad Sci U S A *106*, 3988-3993.

Chu, J., Haynes, R.D., Corbel, S.Y., Li, P., Gonzalez-Gonzalez, E., Burg, J.S., Ataie, N.J., Lam, A.J., Cranfill, P.J., Baird, M.A., *et al.* (2014). Non-invasive intravital imaging of cellular differentiation with a bright red-excitable fluorescent protein. Nat Methods *11*, 572-578.

Dzeja, P.P., Bast, P., Ozcan, C., Valverde, A., Holmuhamedov, E.L., Van Wylen, D.G., and Terzic, A. (2003). Targeting nucleotide-requiring enzymes: implications for diazoxide-induced cardioprotection. Am J Physiol Heart Circ Physiol *284*, H1048-1056.

Dzeja, P.P., Bortolon, R., Perez-Terzic, C., Holmuhamedov, E.L., and Terzic, A. (2002). Energetic communication between mitochondria and nucleus directed by catalyzed phosphotransfer. Proc Natl Acad Sci U S A *99*, 10156-10161.

Fantl, W.J., Johnson, D.E., and Williams, L.T. (1993). Signalling by receptor tyrosine kinases. Annu Rev Biochem *62*, 453-481.

George, S.H., Gertsenstein, M., Vintersten, K., Korets-Smith, E., Murphy, J., Stevens, M.E., Haigh, J.J., and Nagy, A. (2007). Developmental and adult phenotyping directly from mutant embryonic stem cells. Proc Natl Acad Sci U S A *104*, 4455-4460.

Guo, B., Gurel, P.S., Shu, R., Higgs, H.N., Pellegrini, M., and Mierke, D.F. (2014). Monitoring ATP hydrolysis and ATPase inhibitor screening using (1)H NMR. Chem Commun (Camb) *50*, 12037-12039.

Hattori, K., Kajimura, M., Hishiki, T., Nakanishi, T., Kubo, A., Nagahata, Y., Ohmura, M., Yachie-Kinoshita, A., Matsuura, T., Morikawa, T.*, et al.* (2010). Paradoxical ATP elevation in ischemic penumbra revealed by quantitative imaging mass spectrometry. Antioxid Redox Signal *13*, 1157-1167.

Hu, S., Wang, J., Ji, E.H., Christison, T., Lopez, L., and Huang, Y. (2015). Targeted Metabolomic Analysis of Head and Neck Cancer Cells Using High Performance Ion Chromatography Coupled with a Q Exactive HF Mass Spectrometer. Anal Chem *87*, 6371-6379.

Ichikawa, Y., Ghanefar, M., Bayeva, M., Wu, R., Khechaduri, A., Naga Prasad, S.V., Mutharasan, R.K., Naik, T.J., and Ardehali, H. (2014). Cardiotoxicity of doxorubicin is mediated through mitochondrial iron accumulation. J Clin Invest *124*, 617-630.

Imamura, H., Nhat, K.P., Togawa, H., Saito, K., Iino, R., Kato-Yamada, Y., Nagai, T., and Noji, H. (2009). Visualization of ATP levels inside single living cells with fluorescence resonance energy transfer-based genetically encoded indicators. Proc Natl Acad Sci U S A *106*, 15651-15656.

Ingwall, J.S. (2004). Energetics basis for heart failure (SAUNDERS).

Ingwall, J.S. (2009). Energy metabolism in heart failure and remodelling. Cardiovasc Res *81*, 412-419.

527 Jones, D.A., Turner, D.L., McIntyre, D.B., and Newham, D.J. (2009). Energy turnover
528 in relation to slowing of contractile properties during fatiguing contractions of the
529 human anterior tibialis muscle. J Physiol *587*, 4329-4338.
530 Jung, S.H., Kim, K.Y., Lee, J.H., Moon, C.J., Han, N.S., Park, S.J., Kang, D., Song,
531 J.K., Lee, S.S., Choi, M.Y.*, et al.* (2017). Self-Assembled Tb(3+) Complex Probe for
532 Quantitative Analysis of ATP during Its Enzymatic Hydrolysis via Time-Resolved
533 Luminescence in Vitro and in Vivo. ACS Appl Mater Interfaces *9*, 722-729.
534 Kamerlin, S.C., Sharma, P.K., Prasad, R.B., and Warshel, A. (2013). Why nature really
535 chose phosphate. Q Rev Biophys *46*, 1-132.
536 Khlyntseva, S.V., ; Bazel, Ya. R,; Vishnikin, A. B.; Andruch, V. (2009). Methods for the
537 Determination of Adenosine Triphosphate and Other Adenine Nucleotides. journal of
538 analytical chemistry *64*, 657-673.
539 Kolwicz, S.C., Jr., Purohit, S., and Tian, R. (2013). Cardiac metabolism and its
540 interactions with contraction, growth, and survival of cardiomyocytes. Circ Res *113*,
541 603-616.
542 Lacerda, A.E., Kuryshev, Y.A., Yan, G.X., Waldo, A.L., and Brown, A.M. (2010).
543 Vanoxerine: cellular mechanism of a new antiarrhythmic. J Cardiovasc Electrophysiol
544 *21*, 301-310.
545 Laverty, H., Benson, C., Cartwright, E., Cross, M., Garland, C., Hammond, T.,
546 Holloway, C., McMahon, N., Milligan, J., Park, B.*, et al.* (2011). How can we improve
547 our understanding of cardiovascular safety liabilities to develop safer medicines? Br J
548 Pharmacol *163*, 675-693.
549 Lusser, A., and Kadonaga, J.T. (2003). Chromatin remodeling by ATP-dependent
550 molecular machines. Bioessays *25*, 1192-1200.
551 Magistretti, P.J., and Allaman, I. (2015). A cellular perspective on brain energy
552 metabolism and functional imaging. Neuron *86*, 883-901.
553 Mathur, P.P. (1972). Cardiovascular effects of a newer antiarrhythmic agent,
554 disopyramide phosphate. Am Heart J *84*, 764-770.
555 Milberg, P., Reinsch, N., Osada, N., Wasmer, K., Monnig, G., Stypmann, J., Breithardt,
556 G., Haverkamp, W., and Eckardt, L. (2005). Verapamil prevents torsade de pointes by
557 reduction of transmural dispersion of repolarization and suppression of early
558 afterdepolarizations in an intact heart model of LQT3. Basic Res Cardiol *100*, 365-371.

559 Miyazawa, H., Yamaguchi, Y., Sugiura, Y., Honda, K., Kondo, K., Matsuda, F.,
560 Yamamoto, T., Suematsu, M., and Miura, M. (2017). Rewiring of embryonic glucose
561 metabolism via suppression of PFK-1 and aldolase during mouse chorioallantoic
562 branching. Development *144*, 63-73.
563 Nagy, A.G., M.; Vintersten, K.; Behringer, R. (2003). Manipulating the mouse embryo:
564 A laboratory manual. , 3rd edn (1 Bungtown Road, P. O. Box 100, Cold Spring Harbor,
565 NY, 11724-2203, USA: Cold Spring Harbor Laboratory Press).
566 Nakano, M., Imamura, H., Nagai, T., and Noji, H. (2011). Ca(2)(+) regulation of
567 mitochondrial ATP synthesis visualized at the single cell level. ACS Chem Biol *6*, 709-
568 715.
569 Oka, M., Hashimoto, K., Yamaguchi, Y., Saitoh, S.I., Sugiura, Y., Motoi, Y., Honda, K.,
570 Kikko, Y., Ohata, S., Suematsu, M.*, et al.* (2017). Arl8b is required for lysosomal
571 degradation of maternal proteins in the visceral yolk sac endoderm of mouse embryos. J
572 Cell Sci *130*, 3568-3577.
573 Opie, L.H. (2003). Heart Physiology: From Cell to Circulation, 4th edn (LWW).
574 Schimmel, K.J., Richel, D.J., van den Brink, R.B., and Guchelaar, H.J. (2004).
575 Cardiotoxicity of cytotoxic drugs. Cancer Treat Rev *30*, 181-191.
576 Sherlock, S. (1951). The liver in heart failure; relation of anatomical, functional, and
577 circulatory changes. Br Heart J *13*, 273-293.
578 Skou, J.C. (1965). Enzymatic Basis for Active Transport of Na+ and K+ across Cell
579 Membrane. Physiol Rev *45*, 596-617.
580 Strauss, D.G., Gintant, G., Li, Z., Wu, W., Blinova, K., Vicente, J., Turner, J.R., and
581 Sager, P.T. (2019). Comprehensive In Vitro Proarrhythmia Assay (CiPA) Update from a
582 Cardiac Safety Research Consortium / Health and Environmental Sciences Institute /
583 FDA Meeting. Ther Innov Regul Sci *53*, 519-525.
584 Suematsu, M., Suzuki, H., Ishii, H., Kato, S., Hamamatsu, H., Miura, S., and Tsuchiya,
585 M. (1992a). Topographic dissociation between mitochondrial dysfunction and cell death
586 during low-flow hypoxia in perfused rat liver. Lab Invest *67*, 434-442.
587 Suematsu, M., Suzuki, H., Ishii, H., Kato, S., Yanagisawa, T., Asako, H., Suzuki, M.,
588 and Tsuchiya, M. (1992b). Early midzonal oxidative stress preceding cell death in
589 hypoperfused rat liver. Gastroenterology *103*, 994-1001.

590 Sugiura, Y., Katsumata, Y., Sano, M., Honda, K., Kajimura, M., Fukuda, K., and
591 Suematsu, M. (2016). Visualization of in vivo metabolic flows reveals accelerated
592 utilization of glucose and lactate in penumbra of ischemic heart. Sci Rep *6*, 32361.
593 Tantama, M., Martinez-Francois, J.R., Mongeon, R., and Yellen, G. (2013). Imaging
594 energy status in live cells with a fluorescent biosensor of the intracellular ATP-to-ADP
595 ratio. Nat Commun *4*, 2550.
596 Wallace, K.B., Sardao, V.A., and Oliveira, P.J. (2020). Mitochondrial Determinants of
597 Doxorubicin-Induced Cardiomyopathy. Circ Res *126*, 926-941.
598 Wang, L., Jackson, W.C., Steinbach, P.A., and Tsien, R.Y. (2004). Evolution of new
599 nonantibody proteins via iterative somatic hypermutation. Proc Natl Acad Sci U S A
600 *101*, 16745-16749.
601 Wang, Z., Gerstein, M., and Snyder, M. (2009). RNA-Seq: a revolutionary tool for
602 transcriptomics. Nat Rev Genet *10*, 57-63.
603 Watkins, P.B. (2011). Drug safety sciences and the bottleneck in drug development. Clin
604 Pharmacol Ther *89*, 788-790.
605 Yaginuma, H., Kawai, S., Tabata, K.V., Tomiyama, K., Kakizuka, A., Komatsuzaki, T.,
606 Noji, H., and Imamura, H. (2014). Diversity in ATP concentrations in a single bacterial
607 cell population revealed by quantitative single-cell imaging. Sci Rep *4*, 6522.
608 Zala, D., Hinckelmann, M.V., Yu, H., Lyra da Cunha, M.M., Liot, G., Cordelieres, F.P.,
609 Marco, S., and Saudou, F. (2013). Vesicular glycolysis provides on-board energy for fast
610 axonal transport. Cell *152*, 479-491.
611 Zhang, S., Liu, X., Bawa-Khalfe, T., Lu, L.S., Lyu, Y.L., Liu, L.F., and Yeh, E.T. (2012).
612 Identification of the molecular basis of doxorubicin-induced cardiotoxicity. Nat Med *18*,
613 1639-1642.

614

615

616 **ACKNOWLEDGMENTS**

617

618 We thank Mai Samejima and Takashi Musashi for their assistance in cardiac ATP
619 imaging analysis, the members of Motoko Yanagita's laboratory for assistance with
620 experiments and useful discussions, Yoshitaka Ishihara for electroporation**,** Eiichiro
621 Uchino for assistance with data analysis. **Funding:** This work was supported by Grant-
622 in-Aids for Scientific Research (KAKENHI Grant Number 16K09491 to N.K.), the
623 Japan Agency for Medical Research and Development (AMED Grant
624 Number 19gm1210009, JP19gm5010002 and JP19gm0610011); partially by grants
625 from KAKENHI (26293202, 17H04187), Grant in Aid for Scientific Research on
626 Innovative Areas "Stem Cell Agingand Disease (17H05642)", "Lipoquality
627 (18H04673)" (all fonding to M. Yanagita), the JST, PRESTO (JPMJPR14MF), JSPS
628 (KAKENHI Grant Number JP24116703), AMED (Grant Number JP17gm5010002), the
629 Naito Foundation, the Mitsui Life Social Welfare Foundation, the Takeda Science
630 Foundation, the Mother and Child Health Foundation, the Uehara Memorial
631 Foundation, the Japan Brain Foundation, the Nakajima Foundation, the Foundation for
632 Dietary Scientific Research, and the Lotte Foundation (all funding to M.Yamamoto).

633 **Author contributions:** N.K., R.O. and M. Yamamoto designed the experiments. M.

Yamamoto supervised the project. N.K., R.O., R.Y., Y.S., H.A. and M. Yamamoto performed experiments. N.K., R.O., R.Y., Y.S., H.A., S.N. and M. Yamamoto analyzed the data. All authors discussed the results. H. I. and M. Yamamoto wrote the manuscript. **Competing interests**: M.Yamamoto is involved in a pending patent related to GO-ATeam mice. H.I. holds a patent for ATeam probe. All other authors declare no competing interests. **Data and materials availability**: All data is available in the main text or the supplementary materials.

LIST OF SUPPLEMENTARY MATERIALS

KEY RESOURCES TABLE

CONTACT FOR REAGENT AND RESOURCE SHARING

EXPERIMENTAL MODELS AND SUBJECT DETAILS

- Imaging of Muscle Contraction and Measurement of Torque
- GO-ATeam Mouse Model of Myocardial Infarction
- Drug-Induced Cardiotoxicity in GO-ATeam Mice

650 METHOD DETAILS

651 - Cell/Tissue Culture

652 - Embryo Culture

653 - Live Imaging of Embryos

654 - Intravital Imaging of Organs

655 - Metabolome analysis

656 - MS imaging

657 - Organ slices

658 - Image Processing

659 - Measurement of ATP Levels in Mouse Embryonic Fibroblasts (MEFs)

660 - Luciferase Assay

661 - Electroporation

662 QUANTIFICATION AND STATISTICAL ANALYSIS

663 DATA AND SOFTWARE AVAILABILITY

664 SUPPLEMENTAL FIGURE LEGENDS

665

FIGURES & FIGURE LEGENDS

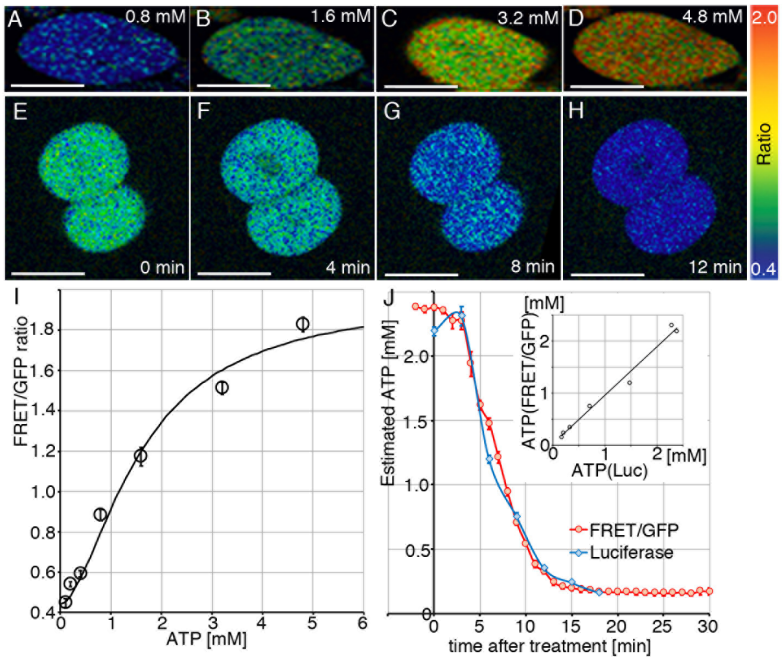

Figure 1

Fig. 1. Measurement of Cytosolic ATP Levels in GO-ATeam transgenic mouse embryos and embryonic fibroblasts

(A-D) Images of FRET/GFP fluorescence emitted by a permeabilized mouse embryonic fibroblasts (MEF) derived from GO-ATeam2 knock-in mouse embryos incubated in calibration buffer. The ATP concentrations in the calibration buffer ranged from 0.8–4.8 mM. There was a close positive correlation between the FRET/GFP ratios and ATP

675 concentrations from 0.1 mM to 6.0 mM (I) (n = 37). The plot was fitted with the Hill

676 equation: $R = (R_{max} - R_{min}) \times [ATP]^n / [ATP]^n + K_d^n) + R_{min}$, where R_{max} and R_{min} are the

677 maximum and minimum fluorescence emission ratios, respectively, K_d is the apparent

678 dissociation constant, and n is the Hill coefficient. (FRET/GFP) = (1.96 – 0.44) ×

679 $[ATP]^{1.7} / ([ATP]^{1.7} + 1.6^{1.7}) + 0.44$.

680 (E-H) FRET/GFP values calculated from images of two-cell embryos treated

681 simultaneously with inhibitors of glycolysis and OXPHOS (2DG and antimycinA,

682 respectively). The ATP concentrations estimated using the FRET/GFP ratio (n = 16)

683 corresponded to those determined using the luciferase assay (J) (n = 118) (inset: R^2 =

684 0.9846). Intensity-modulated display (IMD) images of the FRET/EGFP ratios (0.4 to

685 2.0) are shown. Scale bars indicate 50μm (A-D, I-J), or 25μm (E-H).

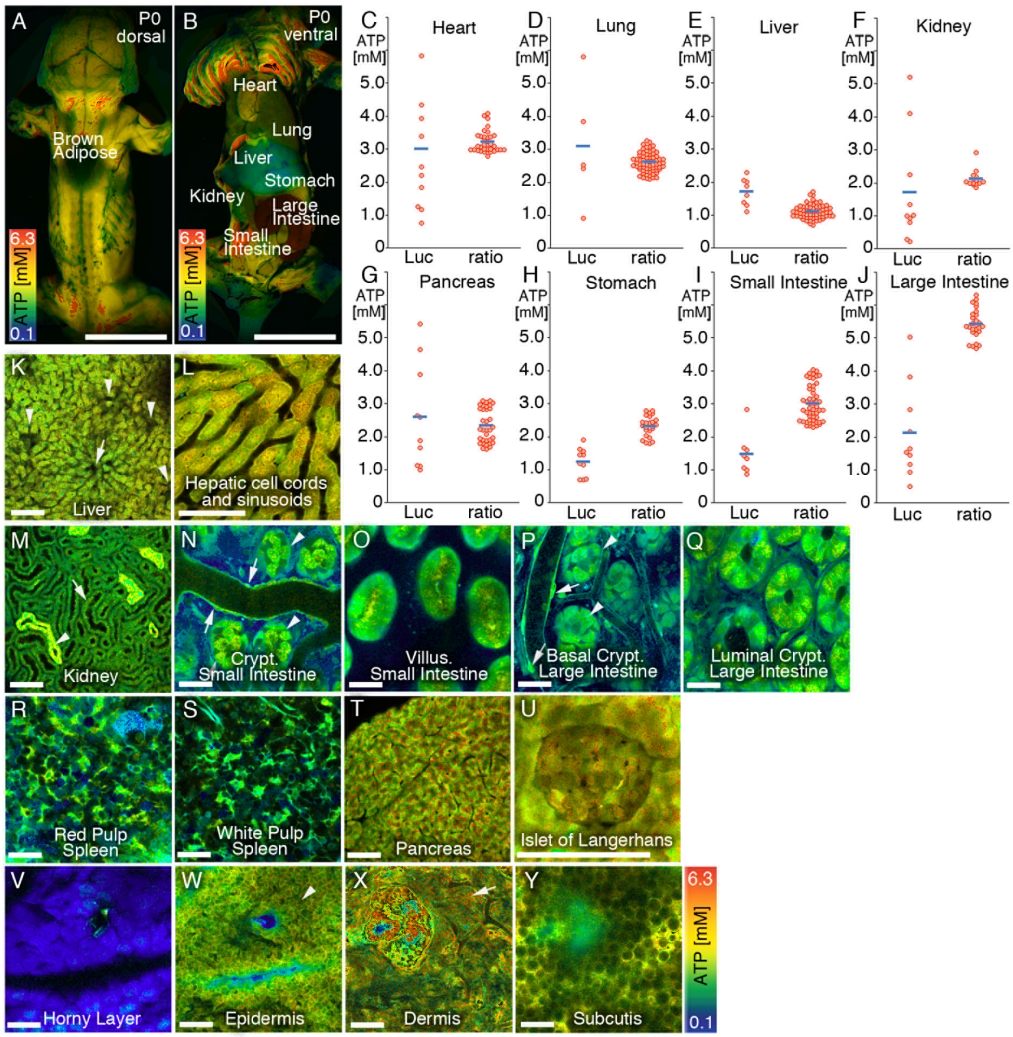

Figure 2

686

687 **Fig. 2. ATP levels in GO-ATeam Live Mice and Intravital Imaging of Organs**

688 (A, B) FRET/GFP fluorescence ratios in postnatal day 0 ([A], dorsal; [B], ventral) GO-

689 ATeam mice.

690 (C–J) ATP concentrations measured using the luciferase assay ("Luc") and FRET/GFP

691 ratios ("ratio") in heart (C), lung (D), liver (E), kidney (F), pancreas (G), stomach (H),

692 small intestine (I), and large intestine (J) in neonatal GO-ATeam mice.

693 (K–Y) Intravital FRET/GFP imaging of an adult (aged 8 weeks) GO-ATeam mouse.

694 Liver (K, L, arrow, central venule; arrowhead, portal venule), kidney (M, arrow,

695 proximal tubule; arrowhead, distal tubule), small intestine (N, O, arrow, blood vessel;

696 arrowhead, paneth cells), large intestine (P, Q, arrow, blood vessel; arrowhead, paneth

697 cells), spleen (R, S), pancreas (T, U), and skin (V–Y, arrow, epidermis; arrowhead,

698 dermis). ATP concentrations (range, approximately 0.1 mM–6.3 mM) are depicted by

699 the spectrum. Scale bars indicate 10mm (A, B), or 100μm (K-Y).

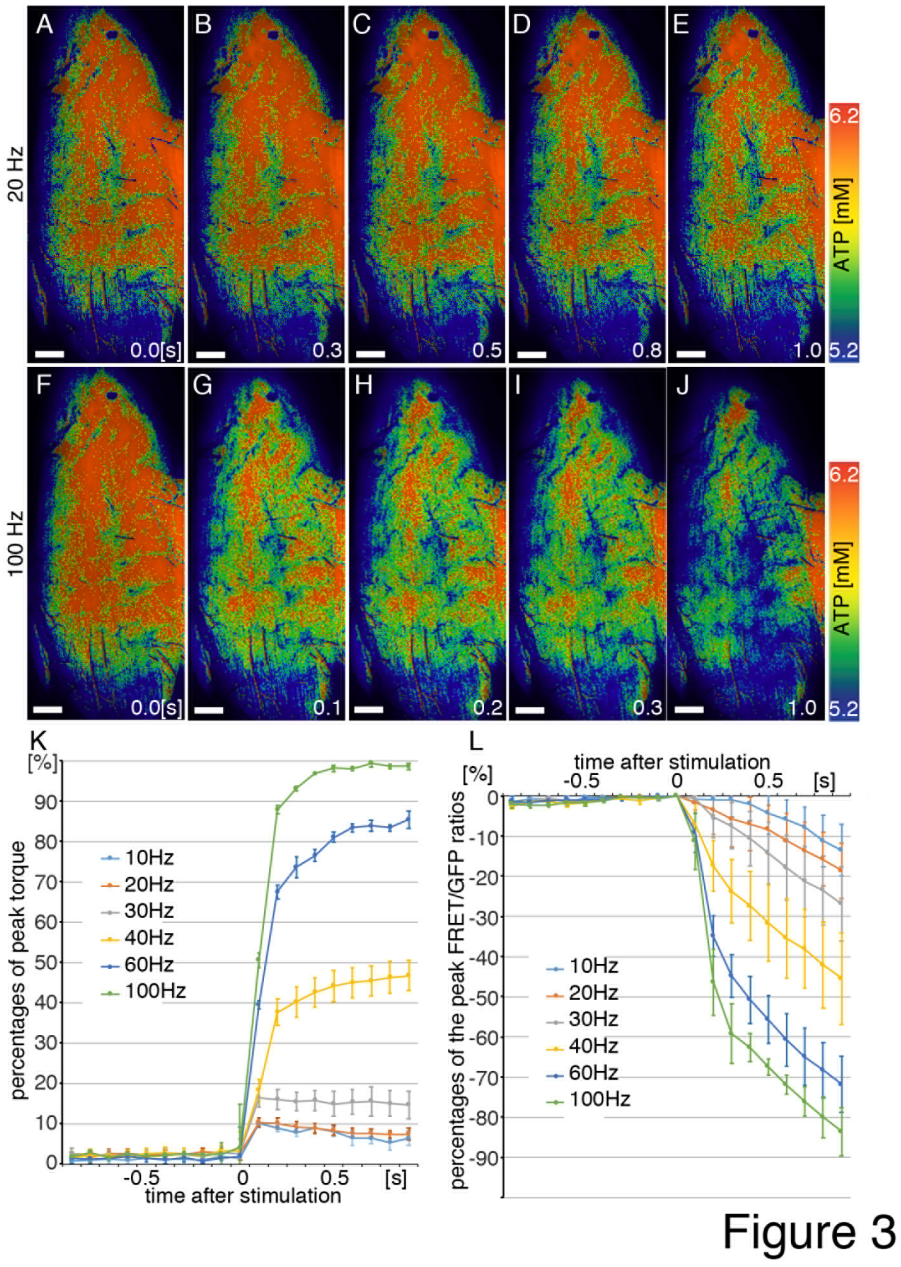

Figure 3

Fig. 3. ATP Dynamics Correspond to the Force Generated by Muscles

Intravital imaging of FRET/GFP ratios of the tibialis anterior muscle subjected to stimulation of the sciatic nerve (A–J). Stimulation frequencies ranged from 20 Hz (A–E) to 100 Hz (F–J). The percentages of peak torque (K) (n = 4) and the percentages of

705 the peak FRET/GFP ratios (L) (n = 4) as a function of time after stimulating the sciatic

706 nerve. The differences between frequency intervals differed significantly (L), except for

707 10 Hz and 20 Hz (K). Numbers indicate seconds after the stimulation, scale bars

708 indicate 100μm (A-J).

709

710

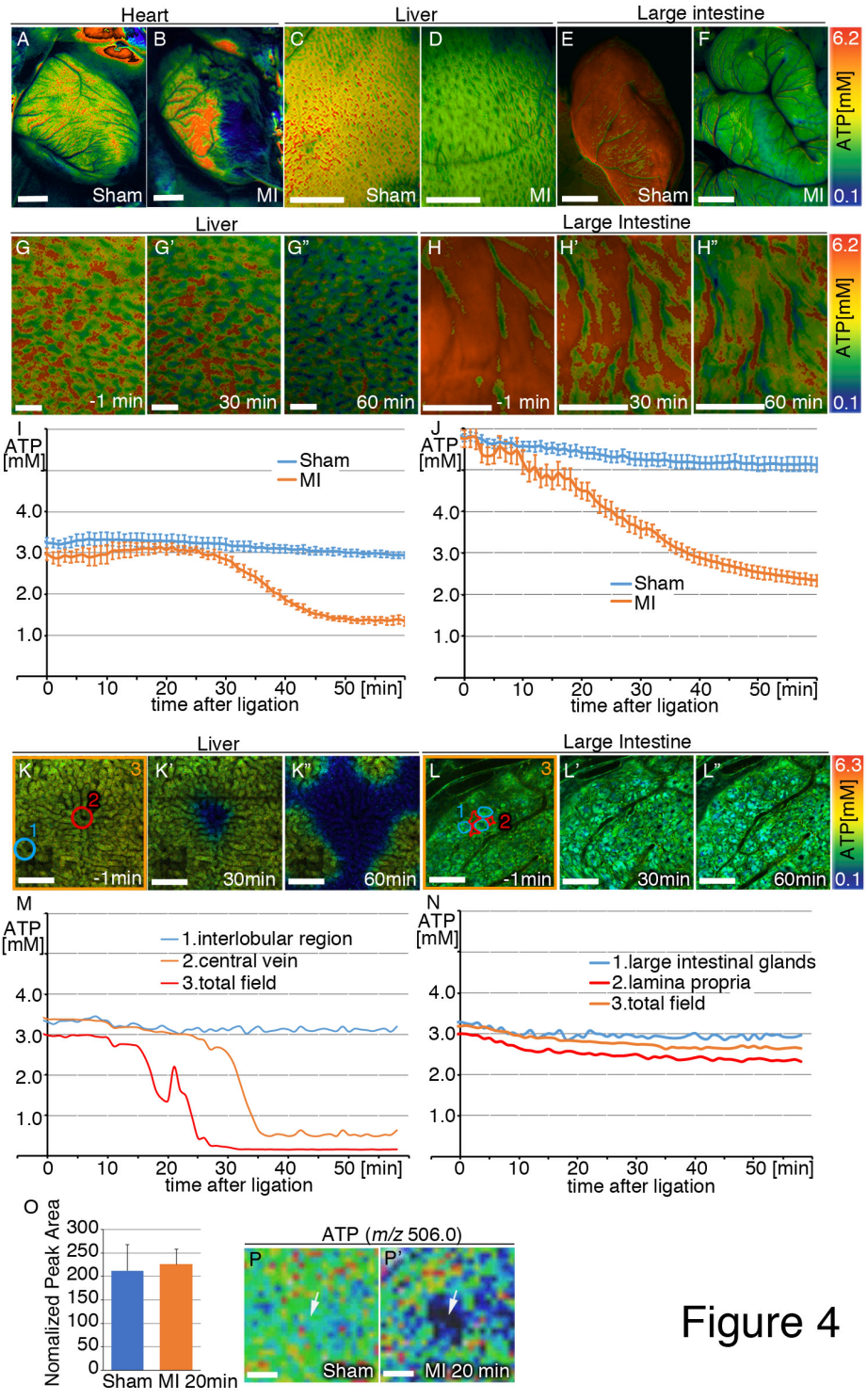

Figure 4

711

712 **Fig. 4. Effects of Myocardial Infarction on ATP Concentrations in the Organs of**

713 **GO-ATeam Mice**

(A–F) Intravital low magnified imaging of FRET/GFP ratios 5 days after ligation of the left anterior descending artery (LAD) (myocardial infarction, MI) (B, D, F; n = 8 each) or sham-operated mice (sham) (A, C, E; n = 8 each). Intravital time-lapse imaging of ATP concentrations calculated from the FRET/GFP ratios in the liver and large intestine using the fluorescence stereo microscope (G–G", H–H"; I [graph of G-G"]; J [graph of H-H"], sham-operated, and MI; n = 9 and n = 6, n = 9 and n = 6, respectively, after t = 31 min; $p<0.05$, after t = 13 min, $p<0.05$) and respective cells using a two-photon microscope (K–K", L–L"; M [graph of K-K"]; N [graph of L-L"]) after ligation of the LAD.

(O-P') Imaging Mass Spectrometry of ATP (*m/z* 506.0) in a sham-operated liver and a liver 20 min after ligation of the LAD (O, P, P': arrow, central vein). In Figs. K and M, the regions of interest (ROIs) 1 to 3 show the periphery of the interlobular region, central vein, and total field of view, respectively. In Figs. L and N, ROIs 1 to 3 show the large intestinal glands, lamina propria, and total field of view, respectively.

Scale bars indicate 2mm (A-F), 1mm (G-H"), or 100μm (K-L", P, P').

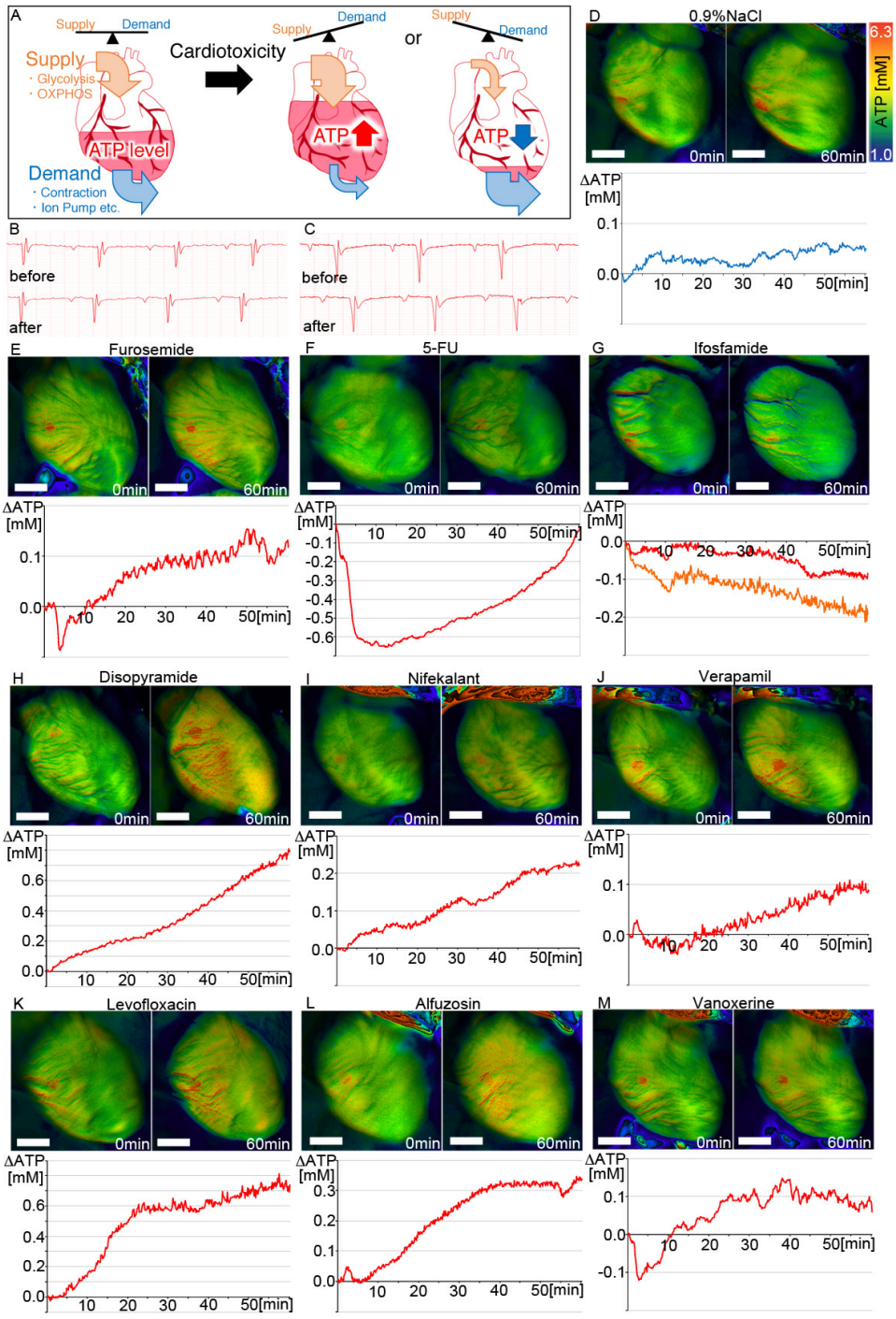

Figure 5

730

731 **Fig. 5. Effects of Drug-Induced Cardiotoxicity on ATP Concentration in the Heart**

732 **of GO-ATeam Mice**

(A) Scheme: Cardiac ATP levels are balanced by supply (glycolysis, OXPHOS, etc.) and demand (contraction, ion pumps, etc.). Due to the drug, cardiotoxicity causes an imbalance between ATP supply and demand, and is expected to alter cardiac ATP levels in a short time. (B, C) electro-cardiogram. The identifier “before” refers to before administration, and “after” refers to 1 hour after administration of the drug, 0.9% NaCl (B) or disopyramide (C). (D-M) Intravital time-lapse imaging of ATP concentrations calculated from the FRET/GFP ratios in the heart using the fluorescence stereo microscope (upper left, before administration; upper right, 60 minutes after administration, with graphical representations shown below each set of panels). The graphs show the change volume in ATP level of whole heart (y-axis) after administration (blue line, 0.9% NaCl; red line, indicated drug; orange line, ifosfamide in left ventricle). Horizontal axis shows time [minutes] after administration. (D) 0.9% NaCl (n=10). (E) furosemide (n=9). (F) 5-FU (n=6). (G) ifosfamide (n=5). (H) disopyramide (n=6). (I) nifekalant (n=6). (J) verapamil (n=6). (K) levofloxacin (n=5). (L) alfuzosin (n=5). (M) vanoxerine (n=4). Scale bars indicate 2mm (D-M).